Cortical Surface Shape Analysis Based on Spherical Wavelets

Peng Yu, *Student Member, IEEE*, P. Ellen Grant, Yuan Qi, Xiao Han, Florent Ségonne, Rudolph Pienaar, Evelina Busa, Jenni Pacheco, Nikos Makris, Randy L. Buckner, Polina Golland, Bruce Fischl*

Abstract—In *vivo* quantification of neuroanatomical shape variations is possible due to recent advances in medical imaging and has proven useful in the study of neuropathology and neurodevelopment. In this paper, we apply a spherical wavelet transformation to extract shape features of cortical surfaces reconstructed from magnetic resonance images (MRIs) of a set of subjects. The spherical wavelet transformation can characterize the underlying functions in a local fashion in both space and frequency, in contrast to spherical harmonics that have a noncompact basis set. We perform principal component analysis (PCA) on these wavelet shape features to study patterns of shape variation within normal population from coarse to fine resolution. In addition, we study the growth of cortical folding pattern in newborns using the Gompertz model in the wavelet domain, allowing us to characterize the order of development of large-scale and finer folding patterns independently. To improve generalization performance, we use a regularization framework to estimate the parameters of the Gompertz model given a limited amount of training data. We develop an efficient method to estimate this regularized growth model based on the Broyden-Fletcher-Goldfarb-Shannon (BFGS) approximation of Hessian matrices. Promising results are presented using both PCA and the growth model in the wavelet domain. The growth model provides quantitative anatomic information regarding macroscopic cortical folding development and may be of potential use as a biomarker for early diagnosis of neurologic deficits in newborns.

Index Terms—folding, MRI, multiscale, neurodevelopment

P. Yu is with the Harvard-MIT Division of Health Sciences and Technology (HST), Massachusetts Institute of Technology (MIT), Cambridge, MA 02139 USA (e-mail: pengyu@mit.edu).

P. E. Grant is Chief of Pediatric Radiology, Massachusetts General Hospital (MGH), Boston, MA 02114 USA and with the Athinoula A. Martinos Center for Biomedical Imaging, MGH/MIT/HMS, Charlestown, MA 02129 USA (e-mail: ellen@nmr.mgh.harvard.edu).

Y. Qi is with the Computer Science and Artificial Intelligence Laboratory (CSAIL), MIT, Cambridge, MA 02139 USA (e-mail: alanqi@csail.mit.edu).

X. Han was with the Athinoula A. Martinos Center for Biomedical Imaging, MGH/MIT/HMS, Charlestown, MA 02129 USA. He is now with the CMS Inc., St. Louis, MO 63132 USA (e-mail: xiao.han@cmsrtp.com).

F. Ségonne was with CSAIL, MIT, Cambridge, MA 02139 USA. He is now with CERTIS Laboratory, ENPC, Paris France (email: segonne@csail.mit.edu)

R. Pienaar is with the Athinoula A. Martinos Center for Biomedical Imaging, MGH/MIT/HMS, Charlestown, MA 02129 USA (e-mail: rudolph@nmr.mgh.harvard.edu).

E.Busa is with the Athinoula A. Martinos Center for Biomedical Imaging, MGH/MIT/HMS, Charlestown, MA 02129 USA (e-mail: evelina@nmr.mgh.harvard.edu).

J. Pacheco is with the Athinoula A. Martinos Center for Biomedical Imaging, MGH/MIT/HMS, Charlestown, MA 02129 USA (e-mail: jpacheco@nmr.mgh.harvard.edu).

N. Makris is with the Athinoula A. Martinos Center for Biomedical Imaging, MGH/MIT/HMS, Charlestown, MA 02129 USA (e-mail: nikos@nmr.mgh.harvard.edu)

R. L. Buckner is with the department of Psychology, Harvard University, Cambridge, MA 02138 USA, the department of Radiology, Harvard Medical School, Boston, MA 02115 USA, and the Athinoula A. Martinos Center for Biomedical Imaging, MGH/MIT/HMS, Charlestown, MA 02129 USA (e-mail: buckner@nmr.mgh.harvard.edu).

P. Golland is with CSAIL, MIT, Cambridge, MA 02139 USA (e-mail: polina@csail.mit.edu).

*B. Fischl is with the Athinoula A. Martinos Center for Biomedical Imaging, MGH/MIT/HMS, Charlestown, MA 02129 USA, HST, MIT, Cambridge, MA 02139 USA, and CSAIL, MIT, Cambridge, MA 02139 USA (phone: 617-726-4897; fax: 617-726-7422; e-mail: fischl@nmr.mgh.harvard.edu).

I. INTRODUCTION

EVIDENCE suggests that morphological changes of neuroanatomical structures may reflect abnormalities in neurodevelopment, or a variety of disorders, such as schizophrenia and Alzheimer's disease (AD). These morphological variations can be characterized by the change of volume, thickness, surface area and shape. Efforts were originally made to verify the relationship between the pathology and the volumetric variation of various neuroanatomical subjects, such as the cerebral cortex, hippocampus and corpus callosum. Recently, a considerable amount of effort has been focused on developing a technique to quantify the changes in the 2D or 3D shape of brain structures, which could potentially lead to more accurate diagnoses, better treatments, and an improved understanding of neurodevelopment.

To accurately study inter-subject shape variations, one would like to find not only an effective shape representation but also a registration method to preserve individual variation while aligning anatomically important structures. Different techniques employed in these two aspects confer merits and disadvantages to various shape analysis methods. One of the earliest techniques developed in this field represented shape by points sampled on the boundary of the object being studied, and the coordinates of the corresponding points on different subjects were directly used as shape features [1], [2]. Cootes *et al.*

extended this method by building the point distribution model, which allows for global scale analysis of shape variation by applying principal component analysis (PCA) to the positions of the boundary points [3]. However, this method depends heavily on the accuracy of the inter-subject registration for group comparison. Subsequently, parametric models were developed to decompose the boundary or surface using Fourier or spherical harmonic descriptors, and to use the decomposition coefficients as shape descriptor [4]-[7]. A drawback of these models is the lack of ability to study local shape variation because of the global support of the basis functions. Another popular method warps a template to individual subjects and studies the deformation field for shape variations [8]-[11]. Although this method is sensitive to the template selection and presents challenges in interpreting and comparing shape differences using the high-dimensional deformation field, a number of interesting shape analysis results have been obtained and more advanced techniques based on it have been developed. Medial axis techniques, originally proposed by Pizer *et al.* and Golland *et al.* in 3D and 2D, respectively, have been applied as a powerful tool for the shape analysis of a variety of subcortical structures [12], [13]. This technique allows for the separate study of the local position and thickness of the object at both coarse and fine levels. Another advantage of medial descriptions is due to the object intrinsic coordinate system, which facilitates the construction of correspondences between subjects and the subsequent statistical analysis. However, a fundamental problem of any skeletonization technique is sensitivity to perturbations in the boundary, which presents a challenge to the further development and application of medial representations.

The difficulties in finding both a good shape presentation and a robust registration method present a challenge to the study of the complex shape of the cortical surface in human beings, which are highly convoluted and greatly affected by neurodevelopment and neuropathy. In order to accurately and efficiently extract shape features and conduct statistical analysis, we develop a procedure to register and normalize cortical surface models, and decompose them using spherical wavelets. The computed wavelet coefficients can be used as shape features to study the folding pattern of cortical surfaces at different spatial scales and locations, as the underlying wavelet basis function has local support in both space and frequency. Using this method, we proposed to study the patterns of shape variation at different spatial-frequency levels by applying PCA in the wavelet domain, and promising results are shown by using synthetic and real data.

Based on this developed spherical wavelets procedure, we also propose to model growth of cortical surfaces from infancy to early adolescence by using the Gompertz function in the wavelet domain. To achieve an optimum generalization performance with a limited amount of training data, which includes a set of MRI scans of newborns and children, a regularization framework is employed. An efficient method is developed to estimate this regularized growth model using BFGS optimization method.

The entire procedure, including MR image preprocessing, spherical wavelet transformation, statistical analysis using PCA,

and the growth model fitting are introduced in detail in the Methods section. Although the entire procedure can be used to analyze both the gray/white matter boundary and gray-matter/cerebrospinal fluid (CSF) boundary, only the gray/white surface, which is a direct reflection of the gyral folding, is used in this paper to exemplify the developed methods. The results of using PCA in detecting the multi-resolutional patterns of shape variation in a nondemented aged population are demonstrated in the Results section. The use of the proposed growth model in detecting the spatial scale and pattern of the growth of the gray/white matter boundary in newborns and children is also presented.

II. METHODS

The automated procedure for conducting shape analysis using spherical wavelet transformation is shown in Fig. 1. The details of each step are introduced in this section. The tools used for preprocessing the cortical surfaces, and the procedures developed to transform the reconstructed cortical surfaces using SPHARM and spherical wavelets are first introduced. Then the procedure developed to study the pattern of shape variations in a population based on the PCA technique is described. Finally, the growth model that is used to study the growth of the cortical folding is also presented.

A. Preprocessing

For decomposing a surface using basis functions defined in the spherical coordinate system, such as spherical wavelets, the surface must be mapped onto a parameterized sphere. In order to carry out any statistical analysis across subjects, correspondence must be established using a registration procedure. A set of automated tools distributed as part of the FreeSurfer package are used to preprocess the data, which includes cortical surface reconstruction, spherical transformation, and spherical registration based on the folding patterns of cortical surfaces [14, 15].

To reconstruct the cortical surfaces, which include the gray/white matter boundaries and gray-matter/CSF boundaries of the left and right hemispheres, the MR images are first registered to a pre-built template in the Talairach space. The image intensity is normalized to remove spatial variations induced by inhomogeneities in the RF field, and used to guide skull stripping and white matter labeling. This white matter segmentation is further refined and cut to generate a single connected mass of each hemisphere. The surface of the labeled white matter of each hemisphere is then tessellated by using 2 triangles to represent each square face of the voxel in the interface between white matter and differently labeled voxels. To generate a more accurate and smoother white matter surface, this tessellation is refined and deformed in the normalized image volume under smoothness and boundary intensity constraints. Furthermore, the white matter surface is deformed outwards to the location in the volume that has the largest intensity contrast between the gray matter and CSF, and refined to generate the pial surface. Finally, topological defects are

automatically detected and corrected for both surfaces to guarantee spherical topology.

Next, the reconstructed cortical surface of each subject is mapped onto a sphere with minimal metric distortion, and then registered in the spherical coordinate system by minimizing an energy functional that is a combination of a topology preserving term, a folding alignment term and a metric preservation term. This alignment enables us to find anatomically corresponding points on the reconstructed cortical surfaces across subjects.

B. Spherical Harmonics (SPHARM)

The common spherical coordinate system established by this procedure allows us to extract shape features using SPHARM and spherical wavelets. As a natural extension of Fourier transformation on the sphere, SPHARM has been demonstrated to be a powerful tool in describing the boundary of objects of spherical topology. In this method, the coordinates $\bar{v}(\theta, \varphi) = (x, y, z)$, $\theta \in [0, \pi], \phi \in [0, 2\pi)$, of a parameterized surface are expressed as the weighted summation of a set of spherical harmonic basis functions of degree l and order m Y_l^m, $-l \leq m \leq l$:

$$\bar{v}(\theta, \varphi) = \sum_{l=0}^{\infty} \sum_{m=-l}^{l} \bar{c}_l^m Y_l^m(\theta, \varphi), \qquad (1)$$

where the coefficients $\bar{c}_l^m$ contain hierarchical shape information. Truncating the spherical harmonics series at different degrees results in object representations at different levels of detail, as shown in Fig. 2. However, SPHARM coefficients cannot indicate the type and location of shape differences due to the global support property of the basis functions. For the purpose of comparison, SPHARM is implemented in this study to decompose the cortical surface as well.

C. Spherical Wavelets

Broadly speaking, a wavelet representation of a function consists of a coarse overall approximation together with detail coefficients that influence the function at various spatial scales and locations. The classical form of wavelet analysis decomposes signals onto a set of basis functions, called wavelets, in which every wavelet is a scaled and translated copy of a single unique function, called the mother wavelet. However, this shift-invariant theory breaks down when representing data sets defined on a bounded surface. The construction of the newly developed spherical wavelets is based on recursive subdivision starting with an icosahedron (subdivision level 0). Denoting the set of all vertices on the mesh before the jth subdivision as $K(j)$, a set of new vertices $M(j)$ can be obtained by adding vertices at the midpoint of edges and connecting them with geodesics. Therefore, the complete set of vertices at the $(j+1)^{th}$ level can be given by $k(j+1) = K(j) \bigcup M(j)$. Next, using an interpolating subdivision scheme (such as the linear scheme and the Butterfly scheme) and a lifting scheme, the scaling functions $\varphi_{j,k}$ defined at level j and node $k \in K(j)$, and the wavelets $\psi_{j,k}$ defined at level j and node $k \in M(j)$ can be constructed. Any function defined on the sphere can be decomposed using the scaling function at ground level 0 and wavelets at all the higher levels. In application, the fast wavelet transformation algorithm developed can carry out the decomposition without explicit constructions of wavelets and scaling functions [16].

The cortical surfaces reconstructed using the procedure described in previous sections are mapped onto a sphere and deformed to align with each other. Therefore, the original position (x, y, z) of each vertex on the cortical surface can be considered as a function defined on the sphere. To transform this coordinate function into the wavelets domain, these coordinates are first interpolated onto a 7th order icosahedron. The coordinate vector $\bar{v} = (x, y, z)^T$, where x, y, z are coordinates on the original surface, is then expanded by a set of spherical wavelet functions and the scaling function at the ground level as

$$\bar{v} = \sum_{k=K(0)} \bar{\lambda}_{0,k} \varphi_{o,k} + \sum_{j=1,...7, k=M(j)} \bar{\gamma}_{j,k} \psi_{j,k}, \qquad (2)$$

where $\bar{\gamma}_{j,k}$ are the 3-dimensional wavelet coefficients at level j, $j = -1, 0, ...7$ and location k, $k \in M(j)$. The highest level used in our study is 7, since the total number of vertices on icosahedron after subdivision 7 is 163842, which is substantially (20% or so) greater than the typical number of vertices used for representing the cortical surfaces from ~1mm isotropic MRI data. The Butterfly technique is used as the interpolating subdivision scheme to improve the smoothness of the wavelets, and a lifting scheme is selected to generate one vanishing moment.

These coefficients can be used as shape features because each of them provides some limited information about both the position and the frequency of the decomposed surface (Fig. 3). In order to make these shape features invariant to rotation, translation and scaling, the coordinate function has to be normalized with respect to a reference coordinate frame. This normalization is initialized by first transforming each surface using the transformation matrix calculated previously for volume Talairach registration during surface reconstruction. The roughly normalized coordinates of corresponding points on all the surfaces under study, where the correspondence is found by the spherical registration, are then averaged to create a new template surface for the second round normalization. Finally, each surface is normalized by finding an optimal linear transformation that minimizes the mean square error of the transformed individual surface and the template.

The resulting normalized wavelet coefficients provide a way to study shape variations hierarchically and locally.

D. Principle Component Analysis (PCA)

Principal Component Analysis is a useful tool in finding patterns in data of high dimension and has been extensively used in the fields of computer vision and image recognition. Based on this technique, methods have been developed to build generative models of shape variation within a single population and used to segment 2D or 3D medical images [17-19]. The basic idea of these approaches is to identify and visualize the

first few principal modes of the variation of the positions of points on the boundary or surface of the dataset.

For example, if $x_i (i = 1, \cdots N)$ is a vector containing shape features, such as the coordinates of the points on the surface calculated for a group of subjects, then any individual shape can be decomposed as:

$$x_i = \bar{x} + \sum_{n=1}^{N} e_n e_n^T (x_i - \bar{x}), \qquad (3)$$

where $\bar{x}$ is the mean of $x_i (i = 1, \cdots N)$, $e_1, \cdots, e_N$ are the eigenvectors corresponding to eigenvalues $\lambda_1, \lambda_2, \cdots, \lambda_N$ of the covariance matrix of x, in decreasing order. This is essentially equivalent to linearly transforming a dataset into a new coordinate system such that the variance of the projection of the dataset on the first axis (first principal component) is greatest, and the variance of projection on the second axis is the second greatest, and so on. The fact that the variance explained by each eigenvector is equal to the corresponding eigenvalue enables us to study the most significant modes of variation in the dataset. Usually, most of the variations can sufficiently be represented by a small number of modes, k, so that the sum of the first k variances represents a sufficiently large proportion of total variance of all the variables used to derive the covariance matrix. Thus by limiting the number of terms in (2), the statistical analysis can be greatly simplified. However, it has been argued that omitting the eigenvectors corresponding to relatively small shape variations leads to the failure of characterizing subtle, yet important shape features because coordinates of all the points on the surface are collected in the shape feature vector [20]. For the same reason, the application of PCA in the shape study of neuroanatomical structures (i.e. the cortical surface) has also been largely limited.

In this work, we propose to conduct PCA on wavelet coefficients at different frequency levels separately, as the coefficients in the lowest level provide an overall approximation and localized morphological variations are captured hierarchically by the higher-level coefficients. Instead of using positions of all the points on the surface as shape features in (3), each time we take only as input $x_{ij} = \{\bar{\gamma}_{j,k}^i | k \in M(j)\}$, the subset of the wavelet coefficients at the jth frequency level. Once the set of principal components $e_{jn} (j = 1, \cdots 7, \ n = 1, \ldots N)$ that characterizes the majority of the variance of the wavelet coefficients in the jth frequency level is found, the corresponding shape variations can be visualized by inversely transforming the principal components to generate the principal surfaces. This visualization technique provides an intuitive way to analyze and understand the most distinct patterns of shape variations within a group of subjects from coarse to fine resolution.

E. Growth Model

The human cortex is highly convoluted, in contrast to the smooth cortex found in other animals such as mice and rats. In human beings, cortical development begins prenatally, and the majority of neurons are generated before birth. The development of cortex folding starts at about 9 weeks in gestation, changes dramatically until birth, but continues into late adolescence. The mechanism involved in the regulated formation of folding pattern remains unclear. It is hypothesized that folding pattern formation is caused by neuron differentiation, migration and the growth of neutrite. Another theory suggests that differential growth of the outer layers relative to inner layer of the cortex results in cortical buckling [21]. A third theory proposed that the mechanical tension generated during the "long-distance" connections of different regions of the brain leads to the formation of folding [22]. Like many growth phenomena in nature, the folding of the human cortex starts slowly, and accelerates before slowing down to approach a limit. In this study, we model the growth of the gray/white boundary at different spatial scales using a growth model in the wavelet domain. Specifically, if $w(t)$ is one of the spherical wavelet features extracted from a subject at age t, we use a Gompertz function to model the features at different ages as follows [23]:

$$w(t) = g_1 \exp(-\exp(-g_2(t - g_3))), \qquad t = T_1, \cdots T_N \qquad (4)$$

where g_1 is the estimated maximum value of the Gompertz model, g_2 is the growth rate, and g_3 is the age of the fastest growth. Given the features, we need to estimate these parameters $\{g_i\}_{i=1,\cdots 3}$.

Due to the limited number of subjects available in this study, a regularization framework is employed for parameter estimation to avoid overfitting. In such a framework, we minimize a cost function

$$Q(b_1, b_2, b_3) = (w(t) - b_1 \exp(-\exp(-b_2 t + b_3)))^2 + c \sum_{j=1}^{3} b_j^2 \qquad (5)$$

$$g_1 = b_1, g_2 = b_2, g_3 = b_3 / b_2$$

where the first term in the right hand side of the equation models the empirical error of model fitting, the second term is a scaled L2 norm regularizer, with the scaling factor c controlling the trade-off between the empirical error and the degree of regularization.

To minimize the cost function Q, we first compute its gradient, which has the closed form:

$$\begin{aligned} \frac{dQ}{db_1} &= \exp(-\exp(-b_2 t + b_3)) \\ \frac{dQ}{db_3} &= -b_1 \exp(-\exp(-b_2 x + b_3)) \exp(-b_2 x + b_3) \\ \frac{dQ}{db_2} &= \frac{dQ}{db_3}(-x) \end{aligned} \qquad (6)$$

Since a simple gradient method suffers from slow convergence, we adopt a quasi-Newton method based on the BFGS approximation of the Hessian matrix [24]. The BFGS method allows us to efficiently minimize f over the parameters $\{b_i\}_{i=1,\ldots 3}$.

We tune the regularization parameter c based on the leave-one-out cross-validation. Specifically, we compute the mean square error of our predictions on the held-out data points using the model parameters optimized from the rest of the training set. From a collection of pre-specified values, we select

the parameter c that minimizes the leave-one-out error. The goodness-of-fit is measured by the R^2, the ratio of the sum of squares explained by the model and the total sum of squares around the mean:

$$R^2 = 1 - \frac{\sum_{i=1}^{N}(\hat{w}(t_i) - w(t_i))^2}{\sum_{i=1}^{N}(\hat{w}(t_i) - \frac{1}{N}\sum_{i=1}^{N}w(t_i))^2} \tag{7}$$

F. Data

Two sets of high-resolution structural MR scans were analyzed in this paper. The first dataset was obtained from a total of 76 nondemented older participants (OP; 55 women: 67 – 95, mean age = 80.45, standard derivation = 7.49; 21 men: 71-90, mean age = 79, standard derivation =6.16). These data have been reported previously in several publications associated with the Washington University Alzheimer's Disease Research Center (ADRC). None of the participants had any history of neurologic, psychiatric, or medical illness that could contribute to dementia or a serious medical condition. Two to four high-resolution MP-RAGE scans were motion corrected and averaged per participant (four volumes were averaged for all except five participants; Siemens 1.5T Vision System, resolution $1 \times 1 \times 1.25$ mm, TR = 9.7 ms, TE = 4 ms, FA = 10 $^\circ$, TI = 20 ms, TD = 200 ms) to create a single high contrast-to-noise image volume. These acquisition parameters were empirically optimized to increase gray/white and gray/CSF contrast. Cortical surfaces were reconstructed and registered as described in previous section. This dataset was mainly used to study normal variations and aging-related shape changes of gray/white matter boundaries in a healthy older population.

The second dataset was from eight normal neonates with corrected gestational ages (cGA) of 30.57, 31.1, 34, 37.71, 38.1, 38.4, 39.72, and 40.43 weeks, and 3 children who were 2, 3 and 7 years old at the time of scanning. T1 weighted 3D SPGR images were collected on a 1.5T scanner, with TR/TE = 30/8, flip angle = 25 to 30 degrees, matrix = 256×192, FOV = 220×165 mm or 200×150 mm and slice thickness 1.2 to 1.4 mm. The images of newborns were manually segmented into white matter and cortical regions due to inverted gray-white contrast and low contrast of the gray-white boundary. The children dataset was processed with automated FreeSurfer tools. Wavelet transformation and growth model are then applied to the reconstructed gray/white matter boundary to study the shape changes of cortical surface in neurodevelopment. To be compared with neonates, children's ages were converted to 167, 235, and 451 weeks by assuming a 40 week gestation period.

III. RESULTS

A. Comparison of Spherical Wavelets with SPHARM

To compare the abilities of SPHARM and spherical wavelets to detect local shape variation, both methods were applied to decompose an inflated cortical surface model with a synthesized shape deformation. The deformed surface was reconstructed using the original surface's coefficients as well as the coefficients calculated from the deformed surface with the most variations, using both SPHARM and spherical wavelets. The coefficient variation is calculated by $\left|\frac{c_d - c_o}{c_o}\right|$, where c_d and c_o are the corresponding coefficients calculated from the deformed and original surfaces respectively. The reconstruction error is measured by $\frac{1}{N}\sum_{i=1}^{N}\left|\bar{x}_r^i - \bar{x}_d^i\right|$, where $\bar{x}_r^i$ and $\bar{x}_d^i$ are the coordinates of the ith vertex on the reconstructed and deformed surfaces, and N is the number of vertices on the surface. Fig. 4(a) is the original surface and Fig. 4(b) shows the set of wavelet coefficients with variation values larger than a prespecified threshold, which accurately localizes the bump around the deformation (indicated by red dots). Conversely, the majority of the SPHARM coefficients have variations larger than the threshold, illustrating the conciseness of the wavelet representation. The synthetic bump is not well reconstructed (Fig. 4(c)), with the 200 most varied SPHARM coefficients, while the deformation is accurately recovered using the same number of coefficients (Fig. 4(d)). A quantitative comparison of the reconstruction error is given in Table I. This type of succinct representation is particularly important to avoid multiple comparison problems that plague the statistical analysis of neuroimaging data.

B. Detection of Shape Variation Using PCA

The PCA study of the wavelet coefficients in the nondemented older sample demonstrated a wide range of differences of cortical surface geometry, in both the overall shape of the cortex and the hierarchically finer local details. Most of the shape variance (98%) was represented by the first 10 to 20 eigenvectors and the variance explained by the first principal component ranges from 8% to 13% of the total variance at the lower spatial-frequency levels. Variances in higher frequency scales spread out more evenly over 50 to 80 eigenvectors. The shape variation represented by the jth principal component at the lth frequency level is illustrated by generating two sets of new wavelet coefficients:

$$x_{j\pm} = \bar{x}_j \pm 3\sigma_{nj}e_{nj}, \tag{8}$$

where $\bar{x}_j$ is the mean wavelet coefficients of all the subjects at j^{th} level, σ_{nj}^2 is the nth eigenvalue of the covariance matrix of the wavelet coefficients at level j. Mean wavelet coefficients were used in the other levels to generate the whole set of wavelet coefficients. By inversely transforming these two sets of wavelet coefficients, two synthetic surfaces can be generated, with the difference between them representing the shape variations characterized by the corresponding eigenvector at different frequency levels. Fig. 5 shows the surfaces generated for levels 0 to 3 with the color indicating the magnitude, location and spatial scale of each coefficient in the first eigenvector e_{j1}. The real surfaces that have the largest positive and negative projections on the first eigenvector are also shown in Fig. 5 to validate the detected shape variations.

Finally, a preliminary study of cortical shape (gray/white matter boundary) variations due to healthy aging was carried out by observing the change with age of the projected surfaces on the set of eigenvectors representing 98% of the variances at each level. The projected surface of the ith subject at the jth level is reconstructed by inversely transforming a new set of wavelet coefficients containing the projected wavelet coefficients on the set of eigenvectors at the jth level, and the mean wavelet coefficients at other levels.

Shape changes consistent with age were observed in the low-frequency domain as well. Fig. 6 shows the projected cortical surfaces in three age ranges of female and male subjects using the second level wavelet coefficients. The narrowing of the central sulcus and the elongation of the occipital lobe with aging were both observed in female and male groups, which may characterize and correlate with white matter atrophy. This result is verified by regressing the projections of all the subjects on the first k principal components (representing 98% of the variances) at each level with age, gender, and other neuropsych measurements. The shape variations detected using PCA are significantly correlated with age at level 0, 2, 4 and 5. More rigorous study will be carried out to clarify the causes of these shape variations.

C. The Growth Study of Gray/White Matter Boundary

In this section we describe the application of the wavelet techniques to detect and characterize the evolution of the folds of the gray/white matter boundary in the neonate and child population described above. We first use the mean squares of all the wavelet coefficients at each frequency level to study the development of folding. As shown in Table II, the R^2 values of the Gompertz growth model fitting at most of the levels are higher than 0.6 in both hemispheres. Furthermore, the estimated age of maximal growth increases, while the estimated growth rate decreases from the low to high frequency levels, indicating that the primary folds develop earlier, but slower than the secondary and tertiary folds. The wavelet power and the predicted growth curves from level 1 to 5 for both hemispheres are shown in Fig. 7.

The growth model was then fitted to each one of the wavelet coefficients across subjects to study the growth of the cortical surface locally at multiple spatial scales. The estimated growth rates and maximum growth ages of the coefficients with R^2 larger than 0.5 are mapped on the youngest newborn cortical surface, as shown in Fig. 8, where the colormap indicates the location and extent of wavelet coefficients selected. The overall changes of the estimated growth rates and maximum growth ages from the low to high spatial scales are consistent with the results from the overall wavelet power growth study. These results provide further characteristics of normal cortical surface growth at different spatial scales and brain regions.

IV. CONCLUSIONS

A spherical wavelet transformation was demonstrated to be able to accurately and efficiently detect the locations and spatial scales of shape variations. The use of wavelet coefficients in detecting and visualizing patterns of cortical surface variation shows promising results in a nondemented aging population. The study of cortical surface growth in newborns also demonstrated the power of wavelets in analyzing the underlying function locally in both the space and the frequency domain. The Gompertz growth function applied to this population was seen to provide a good model for the observed growth as characterized by the wavelet coefficients, and allowed the generation of maps revealing the temporal ordering of the development of large scale and progressively finer scale folds. Future work includes employing more sophisticated statistical tools and extending the wavelet analysis to other neuroanatomical structures.

REFERENCES

[1] I. Dryden and K. Mardia, "Multivariate shape analysis," Sankhya, vol. 55, pp. 460-480, 1993.
[2] F. L. Bookstein, "Morphometric Tools for Landmark Data: Geometry and Biology," 1991.
[3] T. Cootes, C. Taylor, D. Cooper, and J. Graham, "Active shape models - their training and application," Computer Vision and Image Understanding, vol. 61, pp. 38-59, 1995.
[4] C. Brechbüler, G. Gerig, and O. Kübler, "Parametrization of Closed Surfaces for 3-D Shape Description," Computer Vision and Image Understanding, vol. 61, pp. 154-170, 1995.
[5] A. Kelemen, G. Székely, and G. Gerig, "Elastic model-based segmentation of 3d neuroradiological data sets," IEEE Transactions on Medical Imaging, vol. 18, pp. 828-839, 1999.
[6] M. Styner, G. Gerig, J. Lieberman, D. Jones, and D. Weinberger, "Statistical shape analysis of neuroanatomical structures based on medial models," Medical Image Analysis, vol. 7, pp. 207-220, 2003.
[7] L. Shen, Ford J., F. Makedon, and A. Saykin, "hippocampal shape analysis surface-based representation and classification," SPIE Medical Imaging, 2003.
[8] G. Christensen, R. Rabbitt, and M. Miller, "3d brain mapping using a deformable neuroanatomy," Physics in Medicine and Biology, vol. 39, pp. 609-618, 1994.
[9] C. Davatzikos, M. Vaillant, S. Resnick, J. Prince, S. Letovsky, and R. Bryan, "A computerized method for morphological analysis of the corpus callosum," Journal of Computer Assisted Tomography, vol. 20, pp. 88-97, 1996.
[10] S. C. Joshi, M. I. Miller, and U. Grenander, "On the geometry and shape of brain sub-manifolds.," IJPRAI, vol. 11, pp. 1317-1343, 1997.
[11] P. Thompson, J. Giedd, R. Woods, D. MacDonald, A. Evans, and A. Toga, "Growth patterns in the developing brain detected by using continuum machanical tensor maps," Nature, pp. 190-193, 2000.
[12] S. Pizer, D. Fritsch, P. Yushkevich, V. Johnson, and E. Chaney, "Segmentation, registration, and measurement of shape variation via image object shape," IEEE Transactions on Medical Imaging, vol. 18, pp. 851-865, 1999.
[13] P. Golland, W. Grimson, and R. Kikinis, "Statistical shape analysis using fixed topology skeletons: Corpus callosum study," Information Processing in Medical Imaging, pp. 382-388, 1999.

[14] A. M. Dale, B. Fischl, and M. I. Sereno, "Cortical surface-based analysis. I. Segmentation and surface reconstruction," Neuroimage, vol. 9, pp. 179-94., 1999.

[15] B. Fischl, M. I. Sereno, and A. M. Dale, "Cortical surface-based analysis. II: Inflation, flattening, and a surface-based coordinate system," Neuroimage, vol. 9, pp. 195-207, 1999.

[16] P. Schröder and W. Sweldens, "Spherical wavelets: Efficiently representing functions on a sphere," Computer Graphics Proceedings (SIGGRAPH 95), pp. 161-172, 1995.

[17] T. F. Cootes, C. J. Taylor, D. H. Cooper, and J. Graham, "Training Models of Shape from Sets of Examples," Proc. British Machine Vision Conference, Springer-Verlag, pp. 9-18, 1992.

[18] G. Székely and et al., "Segmentation of 2D and 3D objects from MRI volume data using constrained elastic deformations of flexible Fourier contour and surface models," Medical Image Analysis, vol. 1, pp. 19-34, 1996.

[19] M. E. Leventon, W. E. L. Grimson, and O. Faugeras, "Statistical Shape Influence in Geodesic Active Contours," Proc. CVPR'2000, pp. 316-323, 2000.

[20] D. Shen and C. Davatzikos, "An Adaptive-Focus Deformable Model Using Statistical and Geometric Information," IEEE Transactions on Pattern Analysis and Machine Intelligence, vol. 22, pp. 906-913, 2000.

[21] V. S. Jr. Caviness, "Mechanical model of brain convolutional development," Science, vol.189, (4196), pp.18-21, 1975.

[22] D. C. Van Essen, "A tension-based theory of morphogenesis and compact wiring in the central nervous system," Nature, vol. 385, pp. 313--318, 1997.

[23] E. P. Virene, "Reliability Growth and Its Upper Limit," Proceedings of 1968 Annual Symposium on Reliability, pp. 265-270, 1968

[24] C. G. Broyden, Journal of the Institute of Mathematics and Its Applications, vol. 6, pp. 76-90, 1970.
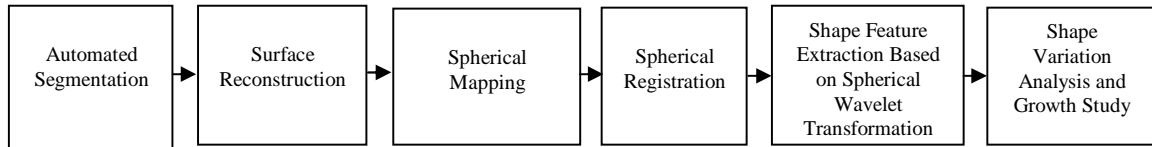
Fig. 1. The automated procedure for conducting shape analysis of neuroanatomical structures.
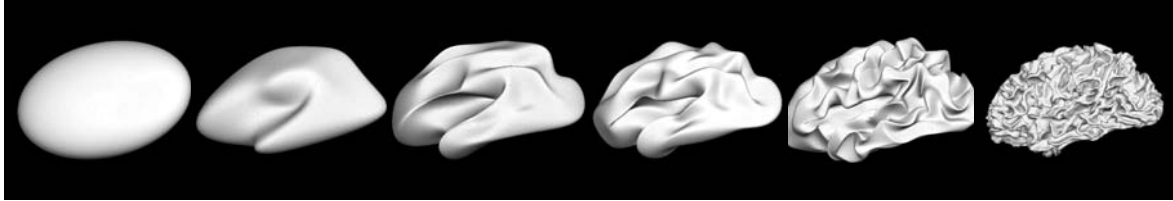
Fig. 2. Reconstructed cortical surfaces using SPHARM coefficients truncated at degree 1, 2, 5, 10, 20, and the original surface.
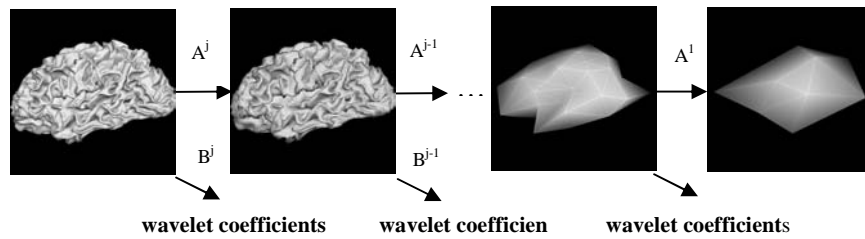
Fig. 3. Wavelet decomposition of cortical surface

(a) **(b)**

(c) **(d)**
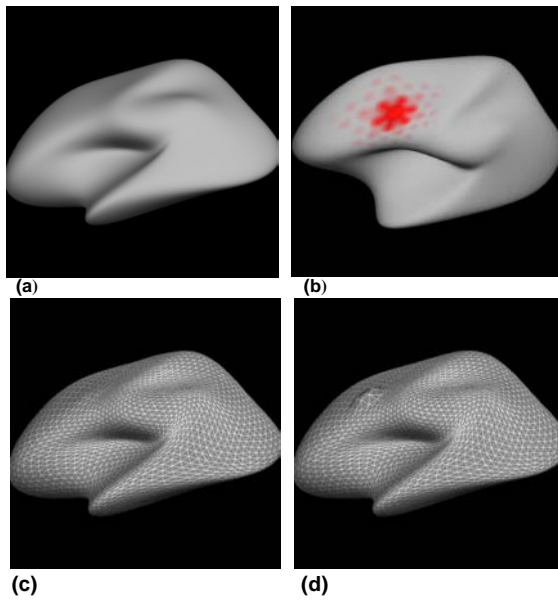
Fig. 4. (a) Original surfaces. (b) The expanded surface with red dots indicating the location of the wavelet coefficients that showed difference from original coefficients. (c) Surface reconstructed with 200 coefficients using SPHARM. (d) Surface reconstructed with 200 coefficients using spherical wavelets

Table I Reconstruction error (%) using varying numbers of coefficient

	10	100	200
SPHARM	96.7	79.3	67.2
Wavelets	57.2	3.55	5.00e-04
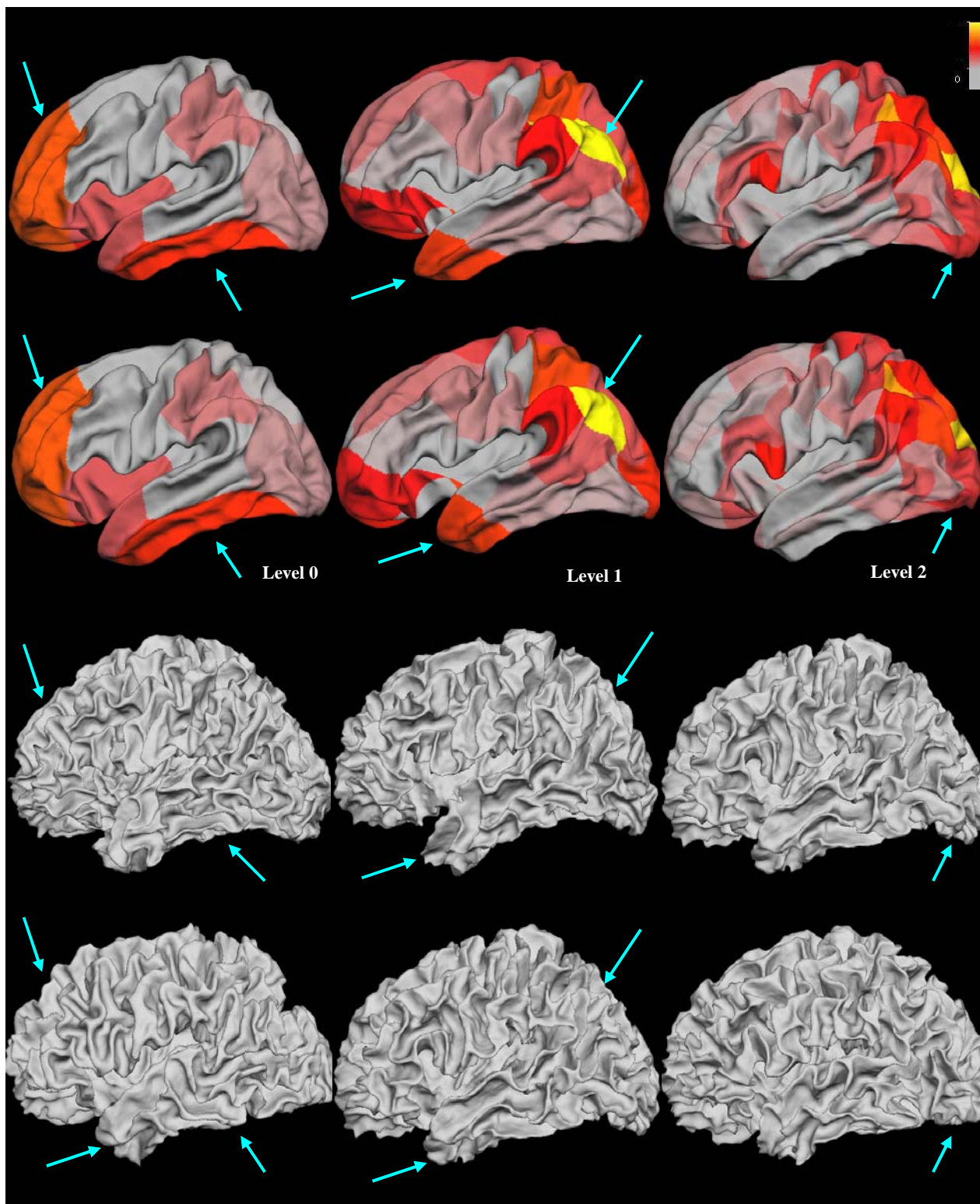
Fig. 5. Top 2 rows: the synthetic surfaces representing the $\mp 3\sigma$ variations (ordered in top-down direction) of the first principal component at level 0 to 3: color showing the spatial scale and magnitude of each wavelet coefficients in the first principle component; Bottom 2 rows: corresponding real surfaces validating the shape variations detected by PCA.
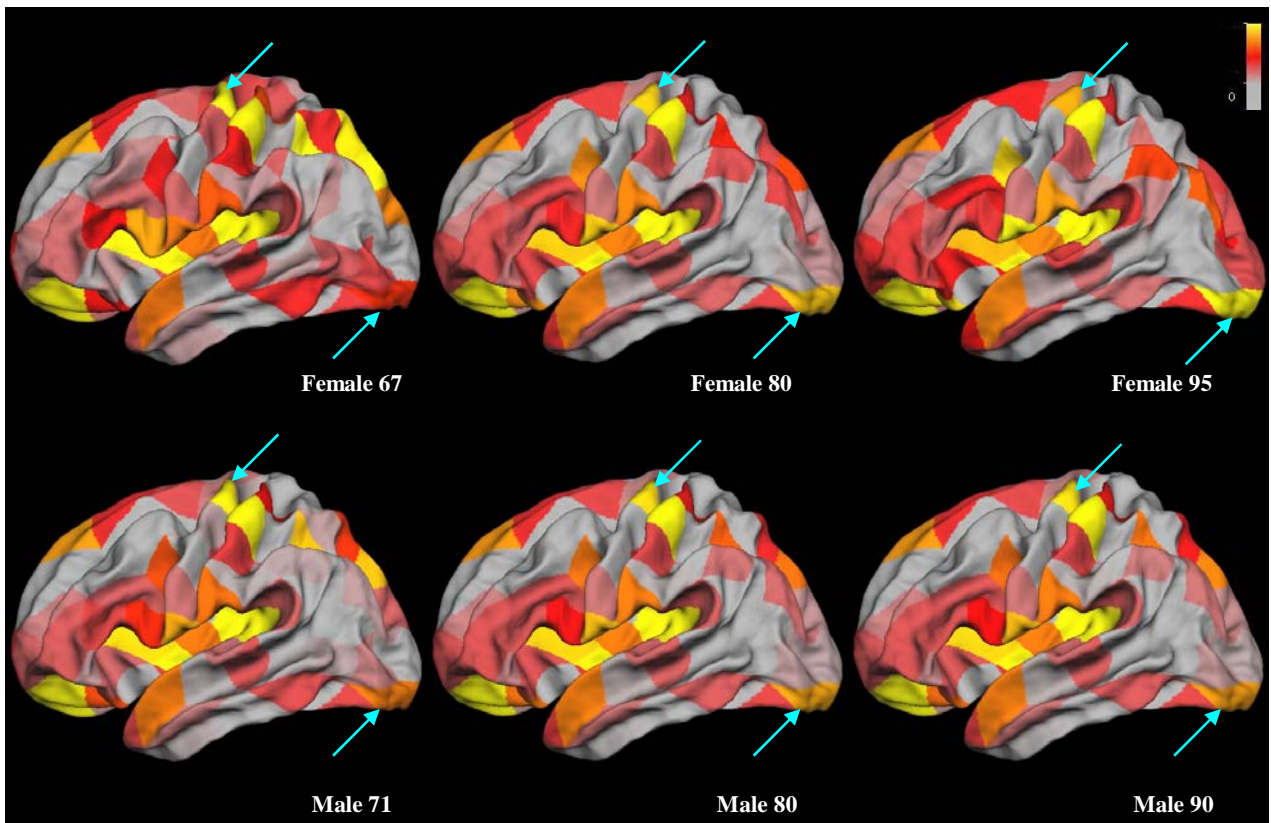
Fig. 6. Reconstructed surfaces for female and male subjects of different ages using projected wavelet coefficients on the set of principal components that represent 98% of the total variance at level 2.
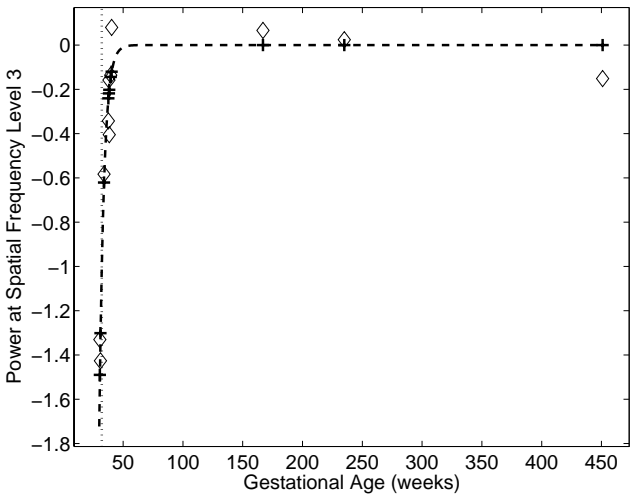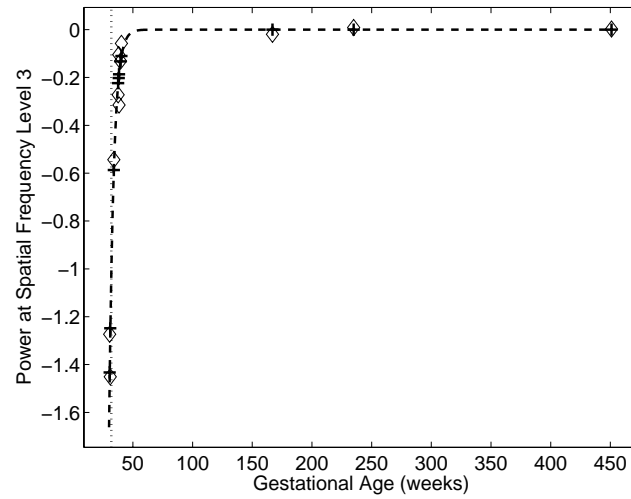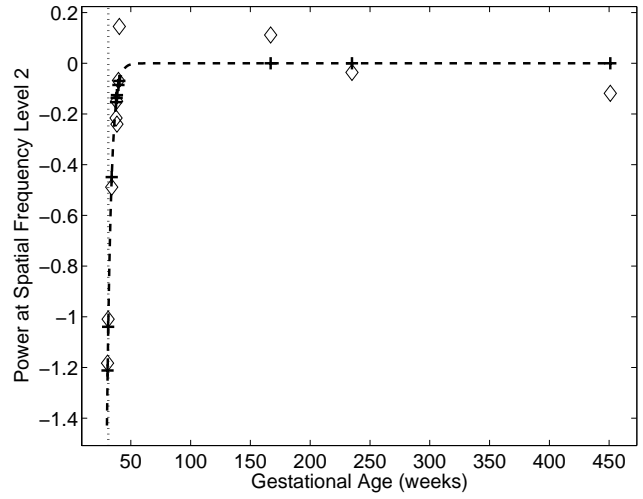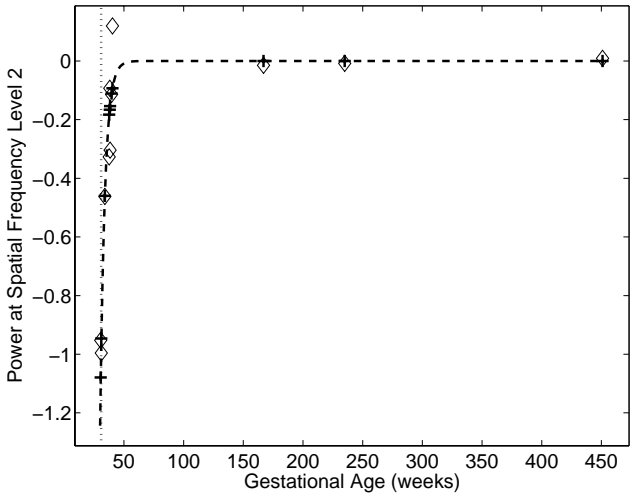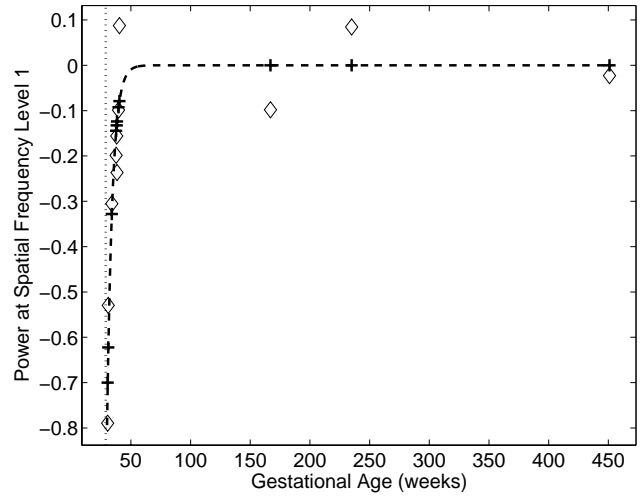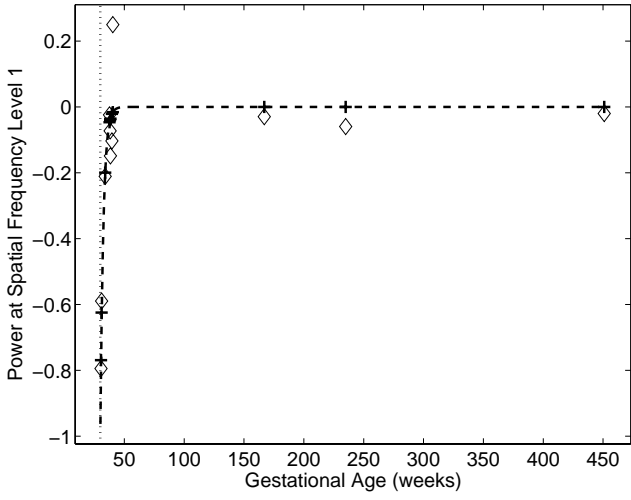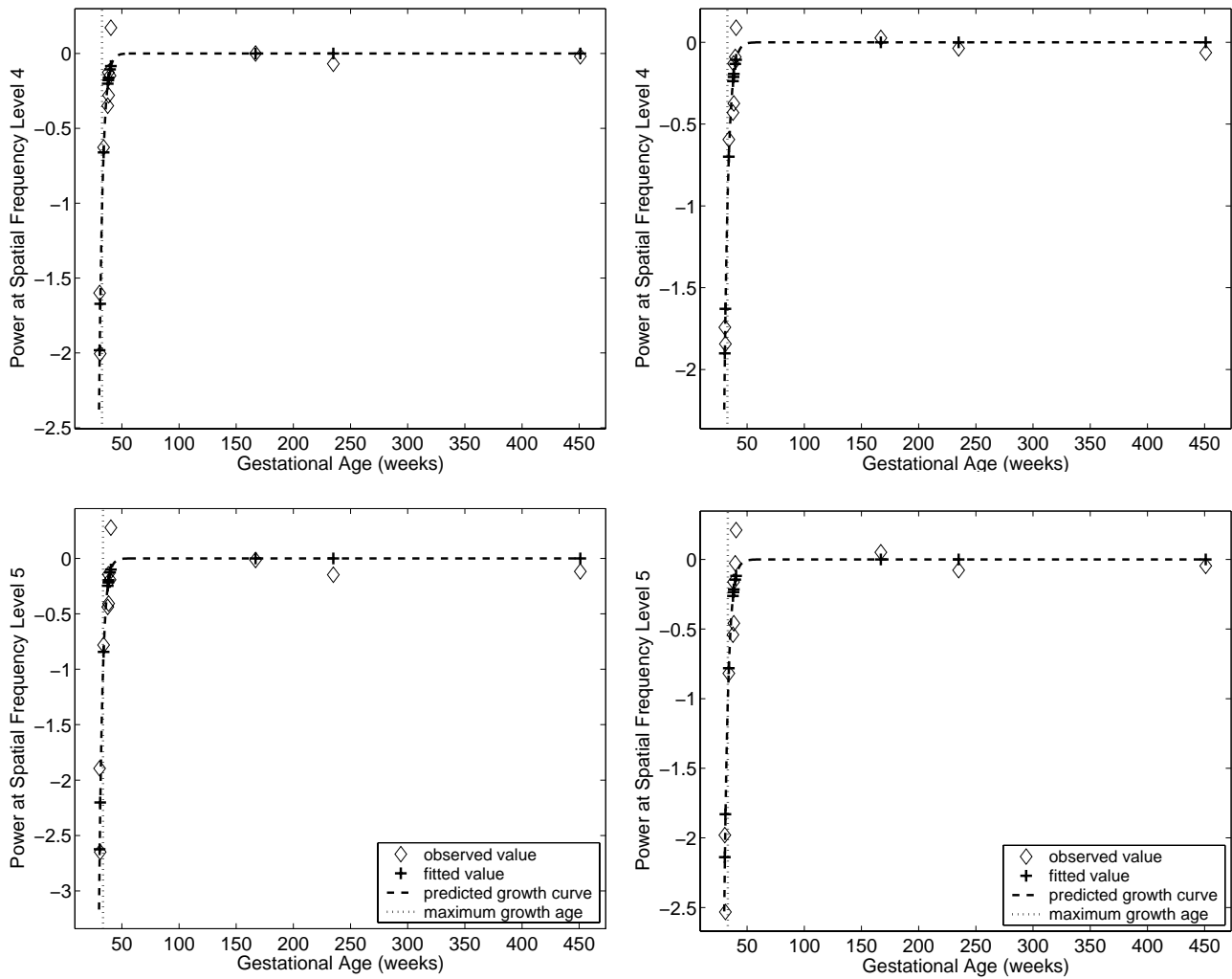
Fig. 7. The predicted growth curves using the mean squares of the wavelet coefficients at levels 1 to 5 for left and right hemispheres (from left to right).

Table II. Growth Model Fitting at Different Frequency Levels For Both Hemisphere

Hemisphere	Level	g1	Growth Rate (1/week)	g3	Maximum Growth Age (week)	R2
	Level 1	72.06308	0.393754	11.77473	29.903736	0.520539
	Level 2	38.88278	0.248656	7.677831	30.877259	0.645357
Left	Level 3	15.43398	0.260217	8.314655	31.95283	0.816203
	Level 4	4.452873	0.32017	10.47158	32.706352	0.684932
	Level 5	0.938141	0.330639	11.07225	33.487467	0.556491
	Level 1	53.10727	0.221013	6.399454	28.955049	0.597591
	Level 2	28.465	0.289463	9.040932	31.233493	0.652711
Right	Level 3	13.65047	0.255177	8.199575	32.132865	0.664997
	Level 4	3.691559	0.291544	9.555109	32.774204	0.702736
	Level 5	0.728441	0.293548	9.733724	33.158875	0.606539
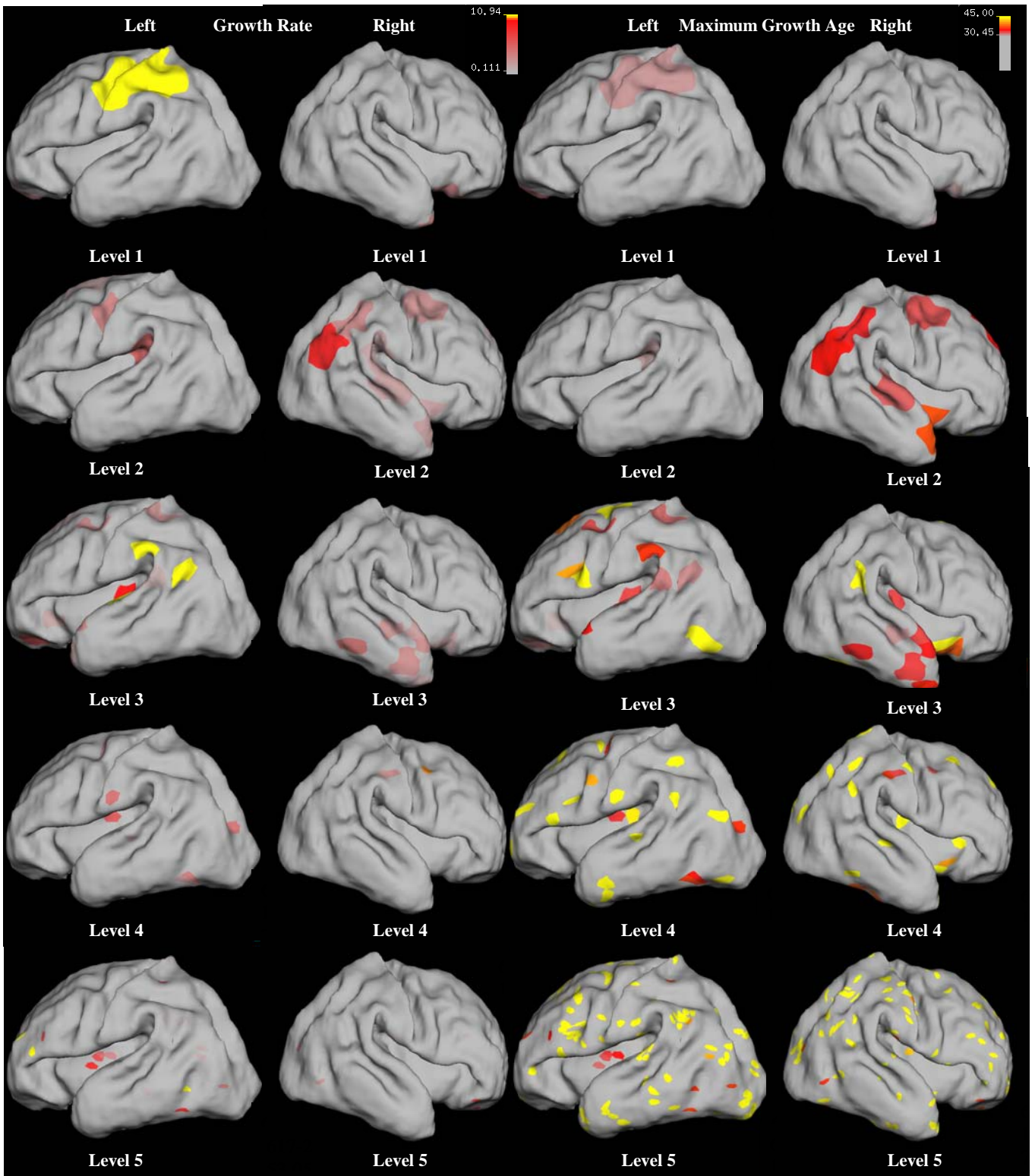
Fig. 8. The predicted growth rate and growth ages for the left and right hemisphere using individual wavelets at level 1 to 5: colormaps indicating the location, spatial coverage and magnitude of estimated growth rate (left; 1/week; scaled up by a factor of 10 for the purpose of illustration) and growth age (weeks; right).